PHOTONIC SENSORS / Vol. 12, No. 1, 2022: 23–30

4-Mercaptopyridine Modified Fiber Optic Plasmonic Sensor for Sub-nM Mercury (II) Detection

Yifan DUAN[1], Yang ZHANG[2*], Fang WANG[1], Yuting SUN[2], Ming CHEN[3], Zhenguo JING[2], Qiao WANG[2], Mengdi LU[2], and Wei PENG[2]

[1]*School of Optoelectronics Engineering and Instrument Science, Dalian University of Technology, Dalian 116000, China*

[2]*School of Physics, Dalian University of Technology, Dalian 116000, China*

[3]*Hebei Institute for Drug and Medical Device Control, Shijiazhuang 050000, China*

[*]Corresponding author: Yang ZHANG E-mail: yangzhang@dlut.edu.cn

Abstract: In this paper, we propose and demonstrate a high-performance mercury ion sensor with sub-nM detection limit, high selectivity, and strong practicability based on the small molecule of the 4-mercaptopyridine (4-MPY) modified tilted fiber Bragg grating surface plasmon resonance (TFBG-SPR) sensing platform. The TFBG-SPR sensor has a rich mode field distribution and a narrow bandwidth, which can detect the microscopic physical and chemical reactions on the sensor surface with high sensitivity without being disturbed by the external temperature. For the environmental compatibility and highly efficient capture of the toxic mercury ion, 4-MPY is modified on the sensor surface forming a stable (4-MPY)-Hg-(4-MPY) structure due to the specific combination between the nitrogen of the pyridine moiety and the Hg^{2+} via multidentate N-bonding. Moreover, gold nanoparticles (AuNPs) are connected to the sensor surface through the (4-MPY)-Hg-(4-MPY) structure, which could play an important role for signal amplification. Under the optimized conditions, the limit of detection of the sensor for mercury ions detection in the solution is as low as 1.643×10^{-10} M (0.1643 nM), and the detection range is 1×10^{-9} M – 1×10^{-5} M. At the same time, the mercury ion spiked detection with tap water shows that the sensor has the good selectivity and reliability in actual water samples. We develop a valuable sensing technology for on-time environmental Hg^{2+} detection and in-vivo point of care testing in clinic applications.

Keywords: Titled fiber Bragg grating; SPR; 4-MPY; mercury ion

Citation: Yifan DUAN, Yang ZHANG, Fang WANG, Yuting SUN, Ming CHEN, Zhenguo JING, *et al.*, "4-Mercaptopyridine Modified Fiber Optic Plasmonic Sensor for Sub-nM Mercury (II) Detection," *Photonic Sensors*, 2022, 12(1): 23–30.

1. Introduction

Mercury is one of the most toxic heavy metal elements in the environment, and it is ubiquitous in the atmosphere, oil, and water resources [1–5]. Mercury in the environment, especially in water, will be enriched and amplified through the aquatic food chain and eventually enter in the human body [6–10]. After entering the human body, mercury ions can bind to many negatively charged groups in enzymes or proteins in the body (such as sulfhydryl group), which affect many metabolic pathways in cells (such as energy generation, protein, and nucleic acid synthesis), thus affecting cell function and growth [11–18]. Mercury is mostly accumulated in the kidney, liver, and brain in the human body. The

Received: 10 October 2020 / Revised: 4 November 2020

DOI: 10.1007/s13320-021-0611-z
Article type: Regular

World Health Organization and the U.S. Environmental Protection Agency clearly stated that the highest mercury content in water that meets the standard is 6 μg/L and 2 μg/L, respectively [19]. Traditional detection methods for mercury ions include inductively coupled plasma mass spectrometry, atomic absorption spectrometry, and atomic emission spectrometry. Although it is possible to accurately measure a variety of metal elements, these methods require complex pretreatment of the sample and the operation processes are usually more complicated. Therefore, it is still necessary to develop a mercury ion detection method with simple operation, and high performance and portability. Currently used mercury ion detection methods are spectroscopic analysis, electrochemical method, and spectrophotometry. In 2015, Zhang *et al.* [20] completed the detection of mercury ions using ultra violet spectroscopy and plasmon resonance technology, with a detection limit of 3.2 nM and a detection range of 4 nM – 40 nM. In 2016, Lu *et al.* [21] used electrochemistry combined with graphene oxide to increase sensitivity to detect mercury ions in water with a detection limit of 0.12 nM and a detection range of 5×10^{-10} M – 5×10^{-8} M. In 2018, Juárez-Gómez *et al.* [22] used spectrophotometry to detect mercury with a limit of detection (LOD) of 7.5×10^{-5} M and a detection range of 5×10^{-5} M – 6×10^{-4} M. The aforementioned methods can basically meet the current demand for the rapid detection of mercury ions, but still have problems such as complicated operation and small detection range, limiting its scope of application. As a new detection method, the fiber optic sensing technology has unique advantages of miniaturization, easy integration, anti-electromagnetic interference, high accuracy, and simple operation, and has been widely used in various applications [23].

Tilted fiber Bragg grating (TFBG) is an exclusive fiber grating based on an optical fiber carrier. Its grating fringe has a certain angle with the fiber normal direction making transfer light couple core modes into the cladding and retaining core mode simultaneously [24]. These exciting cladding modes have rich mode field distribution and extremely narrow bandwidth, and can present different response characteristics to environmental changes, making the TFBG sensor form a good lab-on-fiber sensing platform [25, 26]. By referring to the wavelength and intensity changes of the TFBG fiber core mode, we can eliminate the inherent temperature cross-sensitivity and power dither noise problems during the operation of the sensor and reduce the impact of environmental factors on the sensor spirit detection results. This feature greatly increases the practicability of the TFBG, making it possible to measure targets with the high accuracy in a variety of detection environments. Surface plasma resonance (SPR) technology is currently a practical label-free detection method. It can be combined with a variety of detection structures and has a wide range of applications in biochemical detection [27, 28]. The mercury ion sensor studied in this paper combines the plasmon resonance technology and tilted fiber grating, which can achieve high-precision measurement of mercury ions while retaining the inherent miniaturization, high sensitivity, and temperature interference of the TFBG. The SPR excitation is achieved simply by coating a gold film on the surface of the TFBG. When the gold film surface of the TFBG undergoes microscopic physical and chemical reactions such as the action of biomolecules, the effective refractive index will change, resulting in a change in its cladding mode resonance, that is, a spectral shift.

In this paper, we design and develop a mercury ion sensor by combining the TFBG-SPR sensing technology and 4-mercaptopyridine (4-MPY) molecules with the gold nanoparticle signal amplification method. The 4-MPY molecules are modified both on the surface of the TFBG-SPR and AuNPs through Au-S chemical bonds [29]. When

Hg^{2+} is present, Hg^{2+} will form stable coordination with 4-MPY molecules on the sensor surface and 4-MPY molecules on the surface of AuNPs simultaneously. The bonding, which can connect AuNPs to the sensor surface, can lead to a significant change in the effective refractive index of the TFBG-SPR film, thus achieving the purpose of changing the spectral intensity. In this paper, different water samples are used to test the stability and practicability of the sensor, and the sensor demonstrates the strong reliability, high sensitivity, strong specificity, and wide application range. Fusing the unique structural characteristics of the TFBG, the high sensitivity of the SPR, and the signal amplification characteristics of AuNPs together, this sensor mechanism is suitable for the environmental detection and clinical point of care applications in future.

2. Experiments and method

2.1 Operation principle of sensing system

The key component of the sensor is a 1.5-cm-long TFBG, which is recorded in the core of a standard single-mode fiber (SMF-28 Corning Telecom fiber) by the phase mask method. The optical fiber used in this experiment has undergone hydrogen-carrying treatment in advance to improve its photosensitivity. It is written by a 248 nm ultra-violet (UV) excimer laser pulse (6 mJ, 150 Hz), and the angle between the phase mask and the fiber axis is adjusted. The sensor used in the experiments is a 15° TFBG, and its central wavelength is around 1 550 nm. Then, a 50 nm gold film is sputtered on the sensor surface by magnetron sputtering, so that it generates SPR near the central wavelength of the grating spectrum. In the experimental system, as shown in Fig. 1, a broadband light source with a wavelength range of 1 525 nm – 1 605 nm is used as the input light. Here, in order to effectively excite SPR, we use a polarization controller (PC) to keep the input light in the P polarization state. At the end of the optical path, a spectrum analyzer (OSA, YKAQ6370, Japan) with a wavelength resolution of 0.02 nm is used.

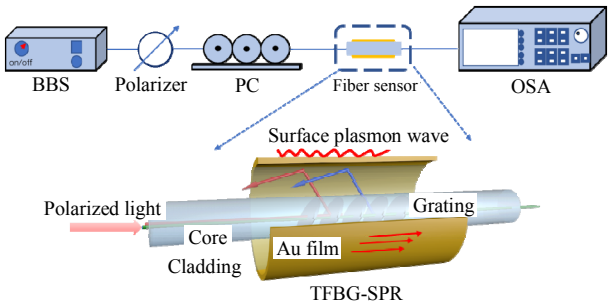

Fig. 1 Schematic illustration of experimental setup for Hg^{2+} detection.

2.2 Materials selection for mercury ion detection

The 4-mercaptopyridine (4-MPY) is purchased from Sigma-Aldrich (Shanghai, China). Sodium citrate (98%) is purchased from Sheng Gong Co., Ltd. (Shanghai, China). Metal salts including Hg^{2+}, Ca^{2+}, Cu^{2+}, Mg^{2+}, Ni^{2+}, and Pb^{2+} are purchased from the Sinopharm Chemical Reagent Co., (Shanghai, China). All of the reagents are of analytical grade. The gold nano colloidal solution used in this article is prepared by the sodium citrate reduction method [30]. This method uses sodium citrate as the reducing agent and protective agent to reduce the Au (III) in $HAuCl_4$ to the atomic state of Au (0). At the same time, the coating ability of sodium citrate itself is used as a protective group, so that the atomic Au is not easily aggregated with other ions, thereby forming gold nanoparticles. In order to provide sufficient coupling power between the deposit nanoparticles and the gold film on the sensor surface and reduce AuNPs' physical adsorption on the sensor surface due to the large particle size, 20 nm AuNPs are selected for modification [31]. For the sensor in this article, 20 nm is much smaller than the depth of the evanescent field on the surface of the TFBG sensor covered with a 50 nm gold film [32]. Therefore, the AuNPs modified on the sensor

surface can play a good role in signal amplification.

In this experiment, the 4-mercaptopyridine and gold nanoparticles and gold film are all linked by Au-S chemical bonds. The surface modification of the sensor is achieved by immersing the TFBG covered with the gold film in the 4-MPY (1 mM) solution overnight. The modified sensors are rinsed with the ethanol solution and deionized water, and then kept in the air. We add 4-MPY (10 μL, 1 mM) to 10 mL of the gold nano colloid solution, stir vigorously for 15 minutes, and then leave it under 4℃ for 12 hours. The modified gold nanoparticles show the structure of AuNPs-(4-MPY). The nitrogen in the 4-MPY molecule can form a stable coordination bond with free mercury ions [29]. In the Hg^{2+} solution, the sensor and the gold nanoparticles are linked together by a (4-MPY)-Hg-(4-MPY) structure as illustrated in Fig. 2(a). In the liquid detection environment where mercury ions exist, gold nanoparticles are modified on the TFBG-SPR sensor. This process affects the TFBG-SPR spectrum, causing it to change in the intensity and wavelength. As shown in Fig. 2(b), AuNPs are modified on the surface of the Au film when the nitrogen in the pyridine part reacts with Hg^{2+}. This process results in a significant change in spectral intensity and wavelength shift towards longer wavelengths. When performing TFBG-SPR sensor signal analysis, a differential technology is usually used [33]. From the spectrum [Fig. 2(b)], it can be seen that the SPR resonance shows a significant amplitude change with the change of the

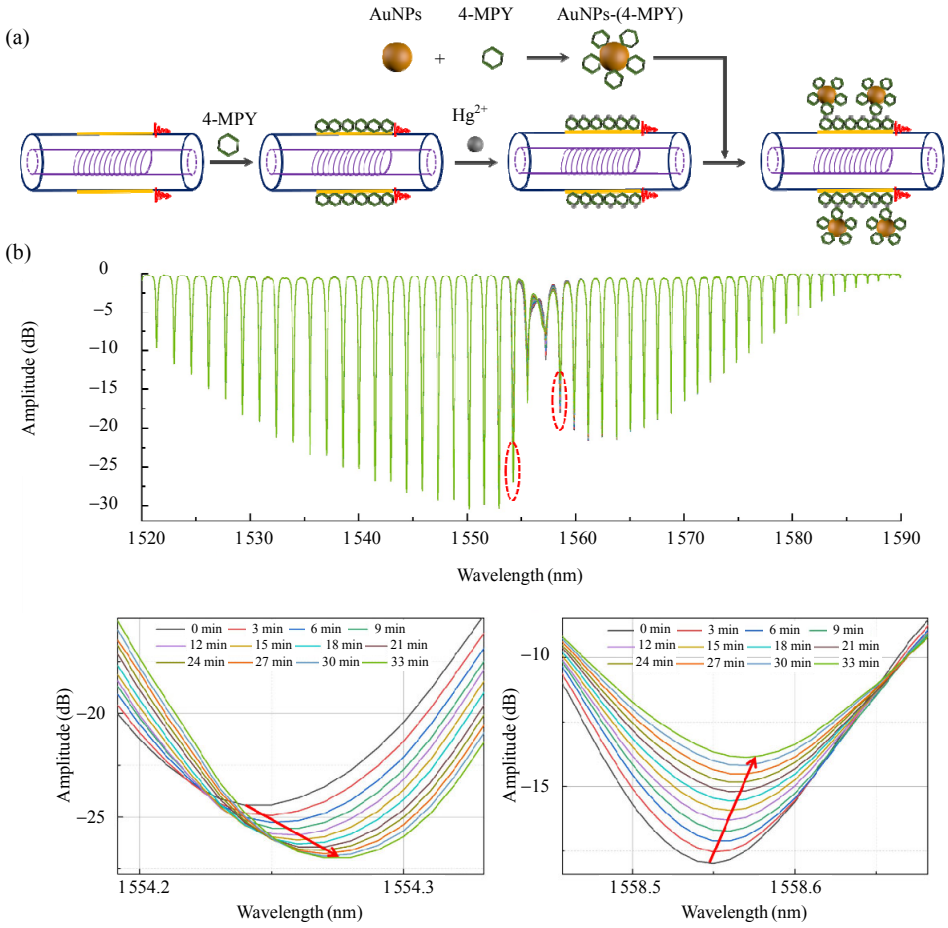

Fig. 2 Self-assembly of 4-MPY on the sensing surface and Hg^{2+} specific identification procedure: (a) schematic diagram of the TFBG-SPR sensing system for detecting mercury ions and (b) spectral response of the TFBG-SPR high order cladding mode.

external refractive index. As shown in Fig. 2(b), the ±1 cladding mode spectrum is generally taken on both sides of the SPR for analysis. It can be seen from the figure that the amplitudes of the two resonance valleys have changed significantly in opposite directions. When evaluating sensor performance, it is necessary to add the amplitude changes of the two wavelengths, and the result obtained corresponds to the spectral response value of the TFBG-SPR under the reaction conditions, making a ~8 000 dB/RIU high sensitivity as reported in [33].

3. Results and discussion

3.1 Chemical reaction and mercury (II) detection

In this experiment, we modify 4-MPY on the gold film surface of the sensor and the free gold nanospheres respectively based on the Au-S chemical bond. Through the (4-MPY)-Hg-(4-MPY) structure, the modified AuNPs are connected to the surface of the TFBG-SPR sensor for signal amplification. As aforementioned, the amplitude variation of TFBG-SPR cladding modes enlarges with the increasing in mercury concentrations. Figures 3(a) and 3(b) show the search engine marketing (SEM) images of the interaction before and after 4-MPY-AuNPs injection. Hg^{2+} forms stable coordination with 4-MPY molecules on the sensor surface and 4-MPY molecules are modified at AuNPs simultaneously. And the AuNPs are captured on the sensing region as indicated in Fig. 3(b). The AuNPs on the sensor surface can significantly change the real and imaginary parts of the surface refractive index of the sensor. This is the main factor that makes the wavelength and intensity of the high-order cladding mode of the TFBG-SPR spectrum change. On the other hand, although the absorbance peak of AuNPs normally is around visible band of 500 nm – 600 nm, some weak LSPR effect still exists in the communication band [34]. Figure 3(c) shows the relationship between the mercury concentration and the signal response of the SPR sensor. This TFBG-SPR biosensor designed based on 4-MPY molecules and AuNPs shows an excellent performance in detecting Hg^{2+} in the range of 1 nM – 10 μM. We conduct five repeated experiments for each concentration and analyze the error of the experimental data to obtain the standard deviation. For the mercury ion sensing system, the final data obtained by this analysis method are relatively accurate and highly reliable. The final calculation limit of detection (LOD) is 1.643×10^{-10} M (0.1643 nM).

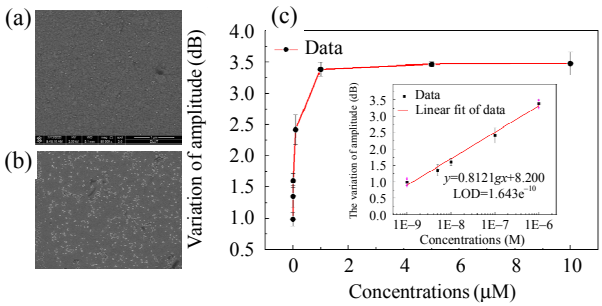

Fig. 3 Detection of mercury ions at different concentrations: (a) SEM images of physical adsorption on the sensing surface, (b) SEM images of AuNPs on the sensing surface after reaction with Hg^{2+} ions at the 100 nM concentration, and (c) spectral amplitude change and sensor detection limit as the concentration of mercury ions changes.

Table 1 Comparison of the LOD and detection range of the biosensor in this paper with other recently reported sensors.

Methods	LOD for Hg^{2+}	Detection range	Ref.
UV spectral-SPR	3.2×10^{-9} M	4×10^{-9} – 4×10^{-8} M	[20]
UV-Vis spectrophotometry	7.5×10^{-5} M	5×10^{-5} – 6×10^{-4} M	[22]
Electrochemical-graphene oxide-DNA	1.2×10^{-10} M	5×10^{-10} – 5×10^{-8} M	[21]
MMF-SPR-AuNPS	8×10^{-9} M	8×10^{-9} – 1×10^{-7} M	[35]
MMF-LSPR-AuNPs	7×10^{-10} M	1×10^{-9} – 5×10^{-8} M	[36]
TFBG-SPR-AuNPs	1.643×10^{-10} M	1×10^{-9} – 1×10^{-5} M	This work

Compared with other methods for Hg^{2+} detection shown in Table 1, our sensor possesses a promising higher sensitivity and larger detection range [20–22, 35, 36]. This biochemical sensor combines the TFBG's miniaturization, portability, temperature resistance, and the ultra-high sensitivity of the SPR sensor. It can accurately measure the mercury ions in the solution, and the detection range can basically

meet the needs of practical applications. It has broad application prospects in environmental water quality testing.

3.2 Sensor selectivity of Hg^{2+} detection

In order to test the selectivity of this chemical sensor, we select several divalent metal ions that exist in actual samples and have relatively similar chemical properties for experiments. The experimental results are shown in Fig. 4. The ion concentration in the experiment is 100 nM. It can be seen from the figure that the detection results of other ions are much smaller than the signal response of Hg^{2+}. Due to the specific combination between the nitrogen of the pyridine moiety and the Hg^{2+}, the stable $Hg(pyridine)_2$ complex is formed via multidentate N-bonding. This feature makes our sensor demonstrate the preferential selectivity toward other divalent metal ions. Therefore, when the actual sample is detected, the concentration of other ions in the sample has no major influence on the Hg^{2+} detection result, and the sensor has certain reliability in practical application.

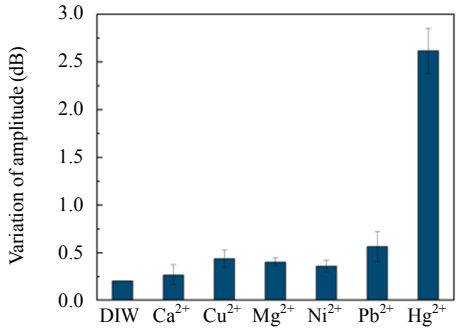

Fig. 4 TFBG-SPR biosensor selectivity for mercury ion detection (all concentrations of Hg^{2+}, Ca^{2+}, Cu^{2+}, Mg^{2+}, Ni^{2+}, and Pb^{2+} are 100 nM).

3.3 Hg^{2+} detection in water samples

To demonstrate the practicability of the 4-MPY modified fiber optic plasmonic sensor for sub-nM mercury (II) detection in the experiment, we carry out a standard addition test on ultrapure water and tap water. The test results are shown in Table 2. Three concentrations of 8 nM, 80 nM, and 800 nM are tested for the two samples. In the ultrapure water sample, by comparing the signal response graph with the logarithmic (log) value of Hg^{2+} concentration, it can be found that the Hg^{2+} concentrations are 7.38 nM, 81.07 nM and 781.37 nM, respectively. And the recovery rates of ultrapure water can be calculated 92.25 %, 101.34 %, and 97.67 %, respectively. In tap water samples, we first detect the background signal response. When the standard Hg^{2+} concentration is 0 in tap water, the calculated Hg^{2+} concentration is 0.407 nM. This result meets the drinking water standard. When other concentrations are tested, the recovery rates of tap water range from 93.08 % to 103.63 %. There is no doubt that this detection result of the sensor has the greater reliability. Therefore, in the detection of actual samples, our designed sensor has the high sensitivity, selectivity, and stability.

Table 2 Hg^{2+} recovery test in ultrapure water and tap water using TFBG-SPR.

Sample	Hg^{2+} added (nM)	Hg^{2+} found (nM)	Recovery (%)
Ultrapure water	8	7.38	92.25
	80	81.07	101.34
	800	781.37	97.67
Tap water	0	0.407	--
	8	8.29	103.63
	80	74.46	93.08
	800	819.96	102.50

4. Conclusions

In summary, this paper presents a high-performance mercury ion sensor with sub-nM LOD, which is based on the tilted fiber Bragg grating surface plasmon resonance sensor modified by the sandwich structure 4-mercaptopyridine. The sensor is miniaturized, resistant to temperature interference inherently, and integrated with the signal amplification effect of gold nanoparticles, and can quickly detect the ultra-low concentration of mercury ions with a large dynamic range. The LOD of the sensor is measured as low as 1.643×10^{-10} M (0.164 3 nM), and the large dynamic detection range is from 1 nM to 10 μM. Using the actual tap water samples for Hg^{2+} measurement, this sensor has high

accuracy and repeatability. Moreover, in drinking water environmental testing, this sensor shows its immunization capability to other metal ions in the water samples. Compared with other Hg^{2+} detection methods, this portable TFBG-SPR mercury ion sensor has lower detection limit, wider detection range, and more compact size, which also possesses of environment temperature self-compensation ability. Due to the high-efficiency, actual in-vivo and time characteristics of this sensor technology, it has potential applications value in clinical and environmental mercury ion detection.

Acknowledgment

Thanks to Huizhen YUAN for the comments provided in the experimental design process. This work was supported by the National Nature Science Foundation of China (Grant Nos. 61520106013 and 61727816), Exchange Fund from Key Laboratory of Optical Fiber Sensing and Communications (Ministry of Education of China) (Grant No. ZYGX2019K006), the Fundamental Research Funds for Central Universities (Grant No. DUT19LAB32), and the Local Science and Technology Development Fund Projects guided by the central government (Grant No. 206Z4801G).

References

[1] J. G. Wiener, D. P. Krabbenhoft, G. H. Heinz, and A. M. Scheuhammer, "Ecotoxicology of mercury, in: handbook of ecotoxicology," *Handbook of Ecotoxicology*, 2003, 2: 439–440.

[2] W. H. Schroeder and J. Munthe, "Atmospheric environment – an overview," *Atmospheric Environment*, 1998, 32(5): 809–822.

[3] S. E. Lindberg, R. Bullock, R. Ebinghaus, D. Engstrom, X. Feng, W. Fitzgerald, *et al.*, "A synthesis of progress and uncertainties in attributing the sources of mercury in deposition," *Ambio*, 2007, 36(1): 19–32.

[4] G. R. Sheu and R. P. Mason, "An examination of methods for the measurements of reactive gaseous mercury in the atmosphere," *Environmental Science & Technology*, 2001, 35(6): 1209–1216.

[5] M. S. Landis, G. J. Keeler, K. I. Al-Wali, and R. K. Stevens, "Divalent inorganic reactive gaseous mercury emissions from a mercury cell chlor-alkali plant and its impact on near-field atmospheric dry deposition," *Atmospheric Environment*, 2004, 38(4): 613–622.

[6] M. Meili, "Fluxes, pools, and turnover of mercury in Swedish forest lakes," *Water Air & Soil Pollution*, 1991, 56(1): 719–727.

[7] O. Lindqvist, K. Johansson, L. Bringmark, B. Timm, M. Aastrup, A. Andersson, *et al.*, "Mercury in the Swedish environment – recent research on causes, consequences and corrective methods," *Water, Air, and Soil Pollution*, 1991, 55(1–2): 1–261.

[8] J. Hua, A. Brun, and M. Berlin, "Pathological changes in the Brown Norway rat cerebellum after mercury vapour exposure," *Toxicology*, 1995, 104(1–3): 83–90.

[9] S. Stine, A. Fredriksson, L. Dencker, and T. Ebendal, "The effect of mercury vapour on cholinergic neurons in the fetal brain: studies on the expression of nerve growth factor and its low- and high-affinity receptors," *Developmental Brain Research*, 1995, 85(1): 96–108.

[10] G. J. Myers and P. W. Davidson, "Prenatal methylmercury exposure and children: neurologic, developmental, and behavioral research," *Environmental Health Perspectives*, 1998, 106(3): 841–847.

[11] M. H. Keating, "*Mercury study report to Congress*," Washington D.C.: Office of Air Quality Planning and Standards and Office of Research and Development, 1997.

[12] IPCS, "International programme on chemical safety, environmental health criteria for methylmercury," Criteria, 101, 1988.

[13] L. Barregard, "Biological monitoring of exposure to mercury vapor," *Scandinavian Journal of Work, Environment & Health*, 1993, 19(1): 45–49.

[14] M. M. Veiga, R. F. Baker, M. B. Fried, and D. Withers, "*Protocols for environmental and health assessment of mercury released by artisanal and small-scale gold miners (ASM)*," Vienna: United Nations Industrial Development Organization, 2003.

[15] E. Rojas, L. A. Herrear, L. A. Poirier, and P. Ostrosky-Wegman, "Are metals dietary carcinogens?," *Mutation Research/Genetic Toxicology and Environmental Mutagenesis*, 1999,

443(1–2): 157–181.
[16] T. Kosatsky, R. Przybysz, B. Shatenstein, J. P. Weber, and B. Armstrong, "Fish consumption and contaminant exposure among Montreal-area sportfishers: pilot study," *Environmental Research*, 1999, 80(2): S150–S158.
[17] L. A. Chapman and H. M. Chan, "Inorganic mercury pre-exposures protect against methyl mercury toxicity in NSC-34 (neuron×spinal cord hybrid) cells," *Toxicology*, 1999, 132(2–3): 167–178.
[18] K. Kramer, J. T. Zoelle, and C. D. Klaassen, "Induction of metallothionein mRNA and proteinin primary murine neuron cultures," *Toxicology and Applied Pharmacology*, 1996, 141(1): 1–7.
[19] T. Thompson, J. Fawell, S. Kunikane, D. Jackson, S. Appleyard, P. Callan, *et al.*, "Chemical safety of drinking water: assessing priorities for risk management," Geneva: World Health Organization, 2007.
[20] Q. L. Zhang, Y. N. Ni, and S. Kokot, "The use of DNA self-assembled gold nano-rods for novel analysis of lead and/or mercury in drinking water," *Analytical Methods*, 2015, 7(11): 4514–4520.
[21] M. H. Lu, R. Xiao, X. N. Zhang, J. H. Niu, X. T. Zhang, and Y. M. Wang, "Novel electrochemical sensing platform for quantitative monitoring of Hg (II) on DNA-assembled graphene oxide with target recycling," *Biosensors & Bioelectronics*, 2016, 85(15): 267–271.
[22] J. Juárez-Gómez, E. S. Rosas-Tate, G. Roa-Morales, P. Balderas-Hernández, M. Romero-Romo, and M. T. Ramírez-Silva, "Laccase inhibition by mercury: kinetics, inhibition mechanism, and preliminary application in the spectrophotometric quantification of mercury ions," *Journal of Chemistry*, 2018, 2018: 1–7.
[23] T. Guo, F. Liu, B. O. Guan, and J. Albert, "Tilted fiber grating mechanical and biochemical sensors," *Optics & Laser Technology*, 2016, 78: 19–33.
[24] C. Caucheteur, V. Voisin, and J. Albert, "Near-infrared grating-assisted SPR optical fiber sensors: design rules for ultimate refractometric sensitivity," *Optics Express*, 2015, 23(3): 2918–2932.
[25] C. Caucheteur, T. Guo, and J. Albert, "Review of plasmonic fiber optic biochemical sensors: improving the limit of detection," *Analytical and Bioanalytical Chemistry*, 2015, 407(14): 3883–3897.
[26] J. Albert, L. Y. Shao, and C. Caucheteur, "Tilted fiber Bragg grating sensors," *Laser & Photonics Reviews*, 2013, 7(1): 83–108.
[27] Y. Zhao, Q. Wang, and H. Huang, "Characteristics and applications of tilted fiber Bragg gratings," *Journal of Optoelectronics and Advanced Materials*, 2010, 12(12): 2343–2354.
[28] X. Y. Dong, H. Zhang, B. Liu, and Y. P. Miao, "Tilted fiber Bragging gratings: principle and sensing applications," *Photonic Sensors*, 2011, 1(1): 6–30.
[29] L. Guerrini, I. Rodriguez-Loureiro, M. A. Correa-Duarte, Y. H. Lee, X. Y. Ling, F. J. Garcia de Abajo, *et al.*, "Chemical speciation of heavy metals by surface-enhanced Raman scattering spectroscopy: identification and quantification of inorganic and methyl-mercury in water," *Nanoscale*, 2014, 6(14): 8368–8375.
[30] K. C. Grabar, R. G. Freeman, M. B. Hommer, and M. J. Natan, "Preparation and characterization of Au colloid monolayers," *Analytical Chemistry*, 1995, 67(4): 735–743.
[31] M. Lu, L. Hong, Y. Liang, B. Charron, H. Zhu, W. Peng, *et al.*, "Enhancement of gold nanoparticle coupling with a 2D plasmonic crystal at high incidence angles," *Analytical Chemistry*, 2018, 90(11): 6683–6692.
[32] C. Shen, W. Zhou, and J. Albert, "Polarization-resolved evanescent wave scattering from gold-coated tilted fiber gratings," *Optics Express*, 2014, 22(5): 5277–5282.
[33] D. Feng, W. Zhou, X. Qiao, and J. Albert, "High resolution fiber optic surface plasmon resonance sensors with single-sided gold coatings," *Optics Express*, 2016, 24(15): 16456–16464.
[34] S. Lepinay, A. Staff, A. Ianoul, and J. Albert, "Improved detection limits of protein optical fiber biosensors coated with gold nanoparticles," *Biosensors and Bioelectronics*, 2014, 52: 337–344.
[35] H. Yuan, W. Ji, S. Chu, Q. Liu, S. Qian, J. Guang, *et al.*, "Mercaptopyridine-functionalized gold nanoparticles for fiber-optic surface plasmon resonance Hg^{2+} sensing," *ACS Sensors*, 2019, 4(3): 704–710.
[36] S. Jia, B. Chao, J. Z. Sun, J. H. Tong, and S. H. Xia, "A wavelength-modulated localized surface plasmon resonance (LSPR) optical fiber sensor for sensitive detection of mercury (II) ion by gold nanoparticles-DNA conjugates," *Biosensors and Bioelectronics*, 2018, 114: 15–21.